Preparation of magnetic graphene photocatalytic nano-adsorbent for the sustainable removal of polycyclic aromatic hydrocarbons from aqueous solution

Qi Ying
University of the Chinese Academy of Sciences School of Chemical Sciences
Taiguang Li
University of the Chinese Academy of Sciences School of Chemical Sciences
Yongmei Hao (ymhao@ucas.edu.cn)
University of the Chinese Academy of Sciences School of Chemical Sciences

Research Article

Keywords: Polycyclic aromatic hydrocarbons (PAHs), Graphene oxide, Adsorption, Photodegradation, Magnetic material□Core-shell structure

Posted Date: June 13th, 2022

DOI: https://doi.org/10.21203/rs.3.rs-1634146/v1

Preparation of magnetic graphene photocatalytic nano-adsorbent for the sustainable removal of polycyclic aromatic hydrocarbons from aqueous solution

Qi Ying, Taiguang Li, Yongmei Hao*

School of Chemical Sciences, University of the Chinese Academy of Sciences, 19(A) Yu Quan Road, Beijing, 100049, China

*Corresponding author at: School of Chemical Sciences, University of the Chinese Academy of Sciences, 19(A) Yu Quan Road, Beijing, 100049, China, PR China. Tel.: +86 10 88256414; fax: +86 10 88256093;

E-mail addresses: ymhao@ucas.ac.cn (Yongmei Hao);

Notes: The authors declare that there is no conflict of interests regarding the publication of this paper.

Highlights

- MGST could be regenerated five times without obvious loss in removal and photolysis efficiency.
- MGST could remove more than 80% of aromatic compounds from coking wastewater and tap water.
- MGST could be applied in the environmental remediation due to its effective enrichment, easy separation, perfect photodegradation activity and sustainability.

Abstract

Magnetic graphene oxide-SiO_2-TiO_2 (MGST) composite was prepared for the absorption and further photodegradation of PAHs to reduce the risk of PAHs in the water environment. Magnetic graphene oxide (MGO) was obtained by introducing Fe_3O_4 to graphite oxide (GO). Furthermore, the suitable SiO_2 layer was wrapped on the MGO for further modification with TiO_2. Finally, the functional MGST composite with uniform morphology was obtained. The prepared MGST was confirmed by XRD, FTIR and XPS, its morphology was observed by SEM and TEM. Naphthalene, phenanthrene and pyrene were selected as models. It was found that the adsorption capacity of MGST showed the order of naphthalene (NAP) < phenanthrene (PHE) < pyrene (PYR). Moreover, the regeneration of MGST was conducted by photolysis, the photodegradation of naphthalene was studied and mechanism was proposed. The successive adsorption-desorption studies indicated that MGST kept its adsorption and photodegradation capability almost constant during 5 cycles, which demonstrated its high stability and good sustainability. Importantly, MGST was able to remove more than 80% of aromatic compounds from coking wastewater and tap water, indicating its promising potential for practical application.

Keywords: Polycyclic aromatic hydrocarbons (PAHs), Graphene oxide, Adsorption, Photodegradation, Magnetic material，Core-shell structure

Introduction

Polycyclic aromatic hydrocarbons (PAHs) are a class of fused-ring organic pollutants. With the rapid development of economy, the ecosystem has been deteriorating severely in recent years and the PAHs have been detected in many water bodies. It is very serious since PAHs can bring damage to people even at very low concentrations. It has strong carcinogenic, teratogenic, mutagenic, as well as phototoxic effects, which causes great harm to both environment and human(Ji et al., 2017; Yang et al., 2018). PAHs have been listed as one of the most critical contaminants by the European Food Safety Authority (EFSA) and the United States Environmental Protection Agency (US-EPA) (Purcaro et al., 2013). Therefore, elimination of PAHs from water source has become one of the research hotspots in environmental science (Chen et al., 2016).

Several technologies, such as bioremediation (Goswami et al., 2018; Gupta et al., 2015), photocatalytic degradation (Yu et al., 2015) and adsorption (Hung et al., 2020; Oliveira et al., 2020; Wickramasinghe and Shukla, 2018), have been applied to the treatment of PAHs in environment. Adsorption with the advantages of low cost, high removal efficiency, facile operation (Ying et al., 2019) and easy regeneration has become a main method for treating PAHs. Recently, biomass adsorbent (Xi and Chen, 2014), mesoporous organosilica (Vidal et al., 2011), metal-organic frameworks (Gao et al., 2016), and various carbon materials (Dappe et al., 2015; Ge et al., 2016; Glomstad et al., 2016; Zhang et al., 2013) have been used to remove PAHs. Compared with other materials, graphene-based adsorbents have encouraging adsorption capacities due to their higher specific surface area and large π-electron system in the plane of the substrate (Huang et al., 2018). Yang et al. used reduced graphene oxide/iron oxide

92 (GO/FeO•Fe_2O_3) composites to absorb PAHs and investigated the adsorption mechanism (Yang
93 et al., 2013). Balati et al. prepared graphene oxide-9-aminoanthracene (GO-9-AA) for PAHs
94 removal (Balati et al., 2017). However, these adsorption processes mainly focus on the
95 enrichment of PAHs and have not eliminated them completely, which may cause secondary
96 pollution.

97 Herein, Fe_3O_4 magnetic graphene oxide-SiO_2-TiO_2 (MGST) was prepared and evaluated as
98 potent adsorbent for PAHs removal. After adsorption, photolysis was applied to degrade the
99 adsorbed PAHs on MGST and regenerate the adsorbent. In order to separate adsorbent from
100 solution easily, Fe_3O_4 magnetic graphene oxide (MGO) is synthesized first since it can be easily
101 separated from the liquid environment by magnetic field without the need for additional
102 procedures (Sheikhmohammadi et al., 2019). As an economical, non-toxic and chemically
103 stable semiconductor, TiO_2 is considered as the most common photocatalyst for the degradation
104 of organic pollutants (Benotti et al., 2009; Shen et al., 2021) and modified on the surface of
105 MGO. However, if TiO_2 nanoparticle connects with magnetic particles directly, its
106 photocatalytic activity will be weakened. This is attributed to the occurrence of Fabry-Perot
107 oscillations when the electrons and holes in TiO_2 are transferred directly to Fe_3O_4 core. Thus,
108 the SiO_2 layer is needed between Fe_3O_4 and TiO_2. Furthermore, it is essential to determine the
109 appropriate amount of SiO_2 while too much SiO_2 can decrease the magnetism of MGST and
110 further weaken the π-π interaction between MGST and PAHs. On the other hand, too less SiO_2
111 will lead to Fabry-Perot oscillations and reduce the photodegradation efficiency.

112 After preparation, adsorption and photodegradation were investigated to evaluate the
113 performance of adsorbent and explore the removal and photodegradation mechanism. The

114 influence of pH and adsorbent dosage on the removal were investigated, both adsorption
115 isotherms and thermodynamics have been analyzed to elucidate the adsorption mechanism. In
116 addition, the photolysis was performed using naphthalene as a model to study the
117 photodegradation mechanism, the efficiencies of regeneration and photodegradation were
118 examined. Finally, MGST has been used to remove naphthalene, phenanthrene and pyrene from
119 real water samples.

120 # 1. Materials and methods

121 ## 1.1 Materials

122 Graphite powder was obtained from Sinopharm Chemical Reagent Co., Ltd. Concentrated
123 H_2SO_4 (98%), $KMnO_4$, HCl (36%), H_2O_2 (30%) solution, absolute alcohol, $FeCl_3 \cdot 6H_2O$,
124 $FeCl_2 \cdot 4H_2O$ and ammonia (25%) were purchased from Beijing Chemical Reagent Company
125 (Beijing, China). Tetrabutyl titanate (TBOT, 97%) and tetraethyl orthosilicate (TEOS, 98%)
126 were the products of Shanghai Macklin Biochemical Co., Ltd. PAHs (naphthalene,
127 phenanthrene and pyrene) were obtained from Sigma-Aldrich. All chemicals used were of
128 analytical grade without further purification in this work.

129 ## 1.2 Characterization

130 Room temperature X-ray diffraction (XRD) data were collected on Rigaku smartlab using
131 Cu Kα radiation over a 2θ range from 20° to 80° at a scanning rate of 10° min-1. Thermo Nicolet
132 360-FTIR spectrometer was used to record FTIR spectra from 400 to 4000 cm-1. Raman spectra
133 were observed from 1000 cm-1 to 1900 cm-1 on a Laser Micro-Raman spectroscope (Renishaw
134 In Via) by using 532 nm laser excitation. The magnetic property of samples were investigated
135 at room temperature by a vibrating sample magnetometer (VersaLab) under an applied field of

30 kOe. X-ray photoelectron spectroscopy (XPS) spectra were collected at room temperature with Thermo ESCALAB 250Xi. The absorption spectra and the concentration of PAHs in aqueous solution were detected by a UV–visible spectrophotometer (UV-2550 SHIMADZU).

1.3 Preparation and characterization of MGST

1.3.1 Synthesis of Fe_3O_4 magnetic graphene oxide (MGO)

Graphite oxide was prepared from nature graphite powder using an improved Hummers method (Marcano et al., 2010), and magnetic graphene oxide (MGO) was synthesized based on our previous method.

1.3.2 Synthesis of MGO-SiO_2 (MGS)

MGO (0.5 g) was dissolved in absolute alcohol (49.5 ml) in a 100 mL flask, the flask was cooled by immersion in an ice-water bath, then some amount of distilled water and TEOS were added. After vigorous stirring for 10 minutes, the ice-water bath was removed. Next to this, 2.0 ml of ammonia was added into the mixture and the mixture was kept stirring at room temperature for 12 h. The product (MGS) was collected using the magnet and washed with absolute alcohol until the supernatant was neutral. The products with different amount of TEOS (the weight ratio of MGO/TEOS is 1: 2, 3, 4, 5, respectively) were labeled as MGS-1 (2, 3, 4 or 5), respectively.

1.3.3 Synthesis of MGS-TiO_2 (MGST)

MGS-4 was selected as the suitable precursor for the synthesis of MGST. MGS-4 (0.2 g) was added to a 500 mL flask containing 200 ml of absolute alcohol and 1 ml of TBOT, and 1.5 mL of H_2O was slowly added into the mixture with vigorous stirring for 30 min. Then, the flask was heated to 60 °C and remained at this temperature for 3 h. After cooling down to the room

158 temperature, the obtained material was washed with deionized water and ethanol three times.
159 Finally, the product was filtrated and freeze-dried. The obtained black powder was MGST.

160 **1.3.4 Characterizations of the photocatalysts**

161 The XRD patterns of synthesized samples are shown in Fig. S1(a). The six characteristic
162 peaks of Fe_3O_4 located at 30.1°, 35.5°, 43.1°, 53.4°, 57.0° and 62.6° can be observed in these
163 samples, which are consistent with the database in JCPDS file (PCPDFWIN v.2.02, PDF No.
164 85-1436). In addition, the XRD of MGST shows two new peaks at 25.25° and 47.98°, which
165 are corresponding to the (101) and (200) planes of TiO_2. FTIR spectra of four samples are given
166 in Fig. S1(b). For the curve a, the broad and strong band in the range of 3500-3200 cm^{-1} relates
167 to O-H stretching vibration. Simultaneously, the peaks at 1724 cm^{-1} and 1225 cm^{-1} are ascribed
168 to the stretching vibration of C=O and C-O-C of epoxy group, respectively. Moreover, the peak
169 appeared at 1616 cm^{-1} should be assigned to the C=C skeletal vibration, while the peaks located
170 at 1049 cm^{-1} and 1350 cm^{-1} are attributed to stretching vibration of C-O and O=C-O groups,
171 respectively (Wang et al., 2009). In the spectrum of MGO, the adsorption peak arising at 552
172 cm^{-1} (Fe-O bond vibration) illustrates the existence of Fe_3O_4 (Junyong et al., 2013). The curve
173 of MGS shows peak at 1055 cm^{-1} which is associated with symmetric vibration of Si-O-Si. In
174 that of MGST (curve d), the peak of 941 cm^{-1} derives from Si-O-Ti vibration, indicating the
175 successful coating of TiO_2 on MGS. Furthermore, the existence of GO in the composite can be
176 detected by Raman Spectroscopy. In Raman spectrum (Fig. S1(c)), the peaks situated at 1350
177 and 1590 cm^{-1} are ascribed to the typical D and G bands of GO. Compared with that of GO,
178 the I_D/I_G value of MGST increases from 0.71 to 0.85, it illustrates the appearance of defects
179 which results from the intruding of Fe_3O_4, SiO_2 and TiO_2 (Yang et al., 2018). This also can be

confirmed by the fact that D peak of MGST has a shift to the higher frequency (blue-shift) compared with that of GO. According to these experimental results, it can be known that MGST was successfully synthesized.

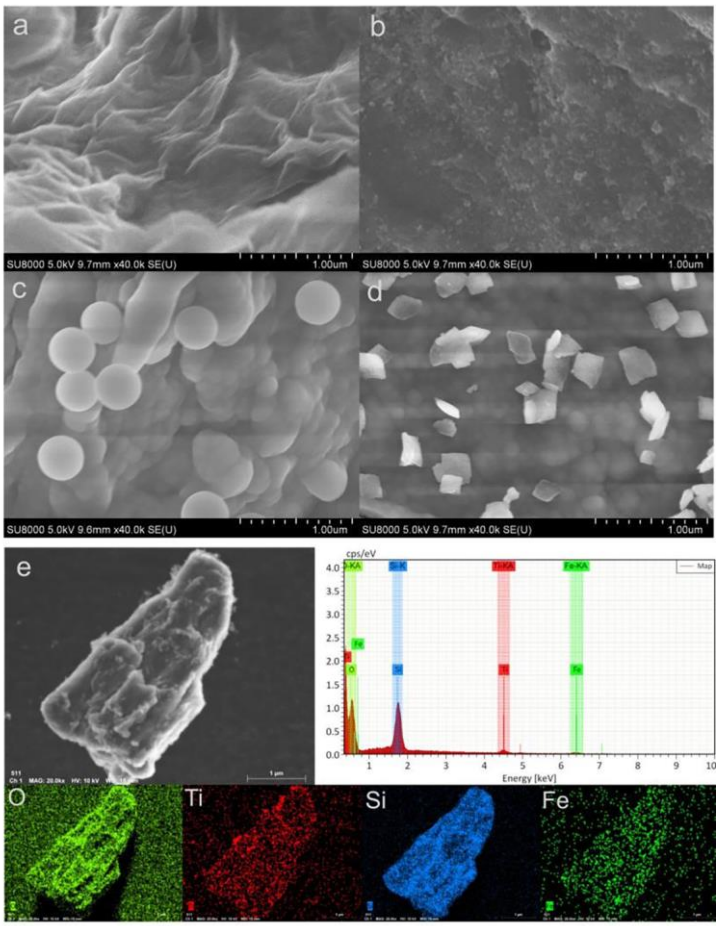

Fig. 1. SEM of GO (a), MGO (b), MGS (c), MGST (d) and EDS mapping images of MGST (e).

SEM image of samples are present in Fig. 1. As depicted in Fig. 1(a), the GO consists of one to several layers. In the image of MGO (Fig. 1(b)), there are small magnetite nanoparticles uniformly scattered on the pleated sheet of GO. After TEOS added in the preparation, it can be clearly seen from Fig.1(c) that SiO_2 spheres are coated onto the MGO. In Fig. 1(d), it shows that TiO_2 nanocubes decorated on MGS, which can be verified by TEM analysis (Fig. 2).

Elemental distribution of MGST can be examined using the elemental mapping, EDS elemental mapping in Fig.1(e) indicates a uniform distribution of O, Ti, Fe and Si elements in the MGST.

In addition, the SEM images of MGS-1 (2,3,4 and 5) are displayed in Fig. S2. From images of MGS-1,2 and 3, it can be clearly seen that the SiO_2 particles coated on MGO were not uniform (Fig. S2(a), (b), (c)), even partial surface of MGO was not covered. While the modification of MGS-4 (Fig. S2(d)) and MGS-5 (Fig. S2(e)) were relatively uniform. Compared with MGS-4, too much SiO_2 particles decorated on the surface of MGS-5, which may lead to reduce in both magnetism and adsorption capacity.

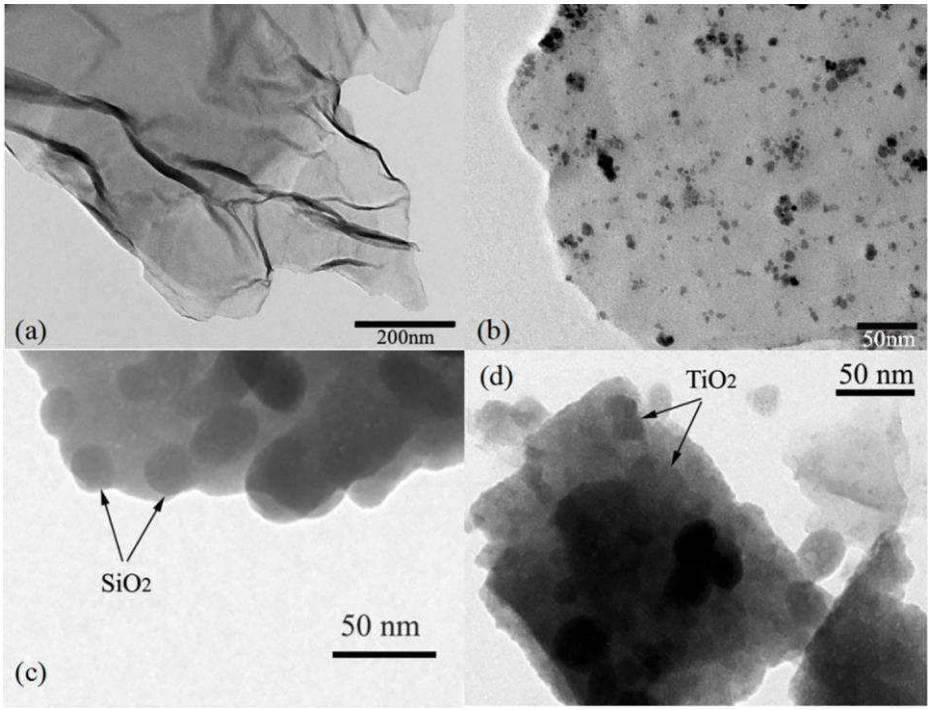

Fig. 2. TEM images of GO (a), MGO (b), MGS (c) and MGST (d).

To further detect the surface composition of MGST, XPS measurement was performed, the relative atomic percentages of the main elements were obtained by XPS analysis and the results are reported in Table S1, the obtained XPS spectrum are shown in Fig. S3. The wide-scan of XPS spectrum (Fig. S3(a)) displays peaks at 103.08, 286.08, 459.08, 532.08 and 711.08 eV, these are ascribed to Si 2p, C 1s, Ti 2p, O 1s and Fe 2p binding energies, respectively. The high-

206 resolution C 1s spectrum of MGST (Fig. S3(b)) shows three peaks at 284.76, 285.83 and 288.38
207 eV, which can be assigned to C-C/C=C, C-O and C=O bonds. Peaks appeared at 724.68 and
208 710.98 eV in Fig. S3(c) correspond to the binding energies of Fe $2p_{1/2}$ and Fe $2p_{3/2}$. The peak at
209 103.08eV (Fig. S3(d)) confirms the existence of SiO_2, and the peaks centered at 458.78eV and
210 464.88eV in Fig. S3(e) are resulted from Ti $2p_{3/2}$ and Ti $2p_{1/2}$ respectively (Zhang et al., 2015).
211 To examine magnetic property, the magnetic hysteresis loops of Fe_3O_4 and MGST were
212 measured and shown in Fig. S3(f). The saturation magnetization intensity of Fe_3O_4 is 72.48
213 emu g^{-1}, while that of MGST is 5.78 emu g^{-1} due to the presence of non-magnetic GO, SiO_2 and
214 TiO_2. However, MGST can still be separated by a magnet within 5 minute and can be re-
215 dispersed with slight shaking, suggesting its potential applications in recycling.

216 **1.4 Adsorption experiments**

217 The adsorption experiments was carried out in a conical flask with 40 ml of PAHs solution
218 and some amount of MGST. The stock solution of PAHs was prepared by dissolved PAHs in
219 methanol, while the working solution was obtained by diluting stock solution with 0.1 mol L^{-1}
220 $CaCl_2$ and simultaneously keeping the volume of methanol less than 0.1% to avoid the
221 cosolvent effect.

222 The pH value was adjusted by 0.1 M NaOH or 0.1 M HNO_3. The concentration of PAHs in
223 the supernatant was measured by a UV-vis spectrophotometer. The removal percentage (%) and
224 the adsorption capacity q_e (mg g^{-1}) can be calculated as follows：

225 $$\text{Removal percentage (\%)} = \frac{C_0 - C_e}{C_0} \times 100\% \quad (1)$$

226 $$q_e = \frac{(C_0 - C_e)V}{m} \quad (2)$$

Where q_e (mg g^{-1}) is the equilibrium amount of PAHs adsorbed on MGST, C_o and C_e (mg L^{-1}) are the initial and equilibrium concentration of PAHs in solution, respectively. V (ml) is the volume of the solution, m (mg) is the mass of MGST.

1.5 Photodegradation and analysis of degradation process

The photodegradation was carried out in a photochemical reaction chamber (CEAULIOHT) which is consist of several 50-ml tubes and a xenon lamp (CEL-LAX, 300 W). The reaction intermediates during photodegradation were analyzed using a GC-MS system (Agilent 7890 A GC with 5975 C Series mass spectrometry) equipped with an Agilent DB EUPAH column (122–5532, 30 m × 250 μ m× 0.25 μm). The oven temperature was programmed from 50 ºC (2 min hold), then increased to 300 ºC (20 ºC·min^{-1}, 5 min hold). EPR spectrometer (Bruker E500) was applied to detect free radicals which were trapped by DMPO at ambient temperature. The operating parameters of EPR were set as follows: center field, 7005 G; sweep width, 14000 G; sample g-factor, 2; microwave frequency, 9.38 GHz; modulation frequency, 100 kHz; power, 0.6325 mW.

2. Results and discussion

2.1. Adsorption

2.1.1. Optimization of MGS

In order to get a suitable amount of SiO_2, we examined the adsorption properties of the MGS. The remove efficiency of seven samples for naphthalene (NAP) (1 mg L^{-1}) are showed in Fig. S4(a). It can be found that the removal capacities of MGO is higher than that of GO. This could be ascribed to the increased layer spacing of GO after modification, the increased layer spacing can accommodate more PAHs molecules. It can be further

249 confirmed by the higher removal efficiencies of MGS than that of MGO. Among all MGS,
250 MGS-1 has the highest removal efficiency, followed by MGS-4. Taking into account the
251 uniformity and thickness of SiO_2 paticles, MGS-4 was chosen as precursor for preparation
252 MGST.

253 **2.1.2. Effect of adsorbent dosage**

254 An optimum adsorbent dose is an essential factor for practical application. To evaluate the
255 optimum dosage, 0.05-0.5 g L^{-1} MGST was added to 40.0 mL of solution containing 1 mg L^{-1}
256 PAHs. As displayed in Fig. 3(a), the removal efficiency of NAP increases from 24 % to 84.63 %
257 with increasing amount of MGST from 0.05 to 0.4 g L^{-1}, the optimum dosage is 0.4 g L^{-1}. On
258 the other hand, the removal efficiency decreased to 78% with addition of 0.5 g L^{-1} MGST. The
259 excessive amount of adsorbent can cause unfavorable agglomeration, thus reduces the effective
260 adsorption sites and causes a decrease in removal efficiency (Hao et al., 2010). Additionally,
261 the removal efficiencies for phenanthrene (PHE) and pyrene (PYR) respectively reach the
262 highest level with 0.2 g L^{-1} and 0.1 g L^{-1} of MGST, and higher than that of NAP. In view of their
263 structure, they have different number of aromatic rings. Since more aromatic rings will have
264 stronger π-π effect, it is reasonable that the optimum amounts of MGST have the trend of PYR<
265 PHE <NAP while the order of removal efficiencies is NAP> PHE> PYR.

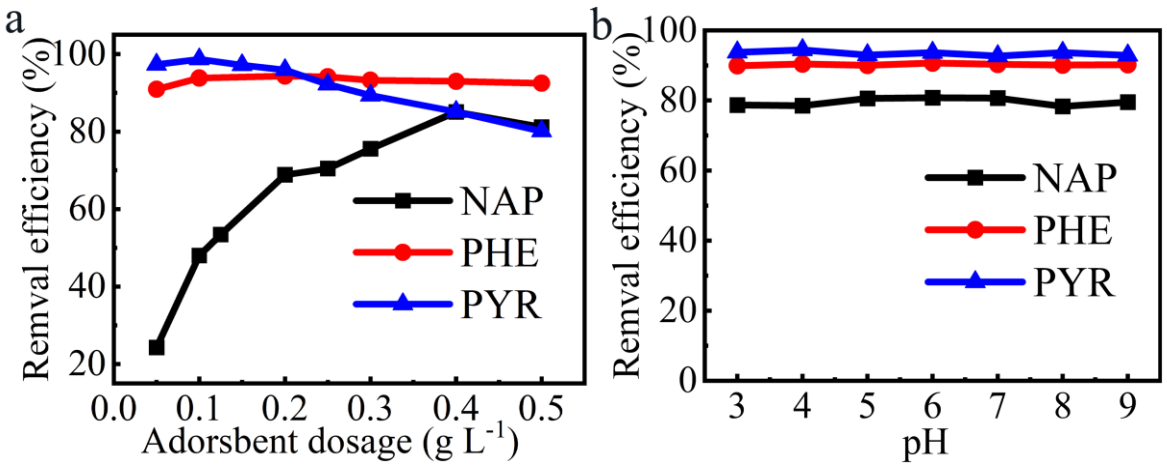

Fig. 3. Effect of adsorbent dosage (a) and pH (b) on the adsorption of PAHs. The experiments were conducted at 1 mg L^{-1} of PAHs and 25 ºC.

2.1.3. Effect of pH on adsorption

The effect of solution pH is another significant factor that needs to be investigated. The adsorption of NAP, PHE and PYR on MGST over the pH range of 3.0-9.0 is presented in Fig. 3(b), it seems that the acidity has no evident effect on the adsorption. The removal efficiency almost keeps constant in the examined pH range. This result is consistent with the adsorption of NAP on graphite and rGOs (Sun et al., 2013).

2.1.4. Comparison of MGST with precursors

The adsorption capacity of various samples was evaluated using NAP as model. From Fig. S4(b), it is clearly seen that the removal capacity of MGO, MGS and MGST are higher than that of GO and MGS shows the best performance. It is speculated that the presence of TiO_2 on the surface may weaken π-π interaction between NAP and adsorbent, which leads to the lower adsorption capacity of MGST than that of MGS.

2.1.5. Adsorption isotherms

To understand the adsorption of PAHs on MGST, Langmuir and Freundlich isothermal models were applied to analyze the experimental data. These two models can be expressed by the following equations

$$\frac{C_e}{q_e} = \frac{1}{K_L q_m} + \frac{C_e}{q_m} \quad (3)$$

$$\ln q_e = \ln K_F + \frac{1}{n} \ln C_e \quad (4)$$

Where q_m represents the maximum monolayer adsorption capacity of adsorbent and K_L (L mg^{-1}) is the Langmuir adsorption constant. Moreover, the type of the Langmuir isotherm can be predicted if the adsorption is favorable or unfavorable based on the dimensionless constant R_L which is defined as follows:

$$R_L = \frac{1}{1 + K_L C_0} \quad (5)$$

The R_L describes the type of isotherm to be irreversible ($R_L = 0$), favorable ($0 < R_L < 1$), linear ($R_L = 1$) or unfavorable ($R_L > 1$). In this study, the values of R_L varying from 0.6750 to 0.8762 suggests a favorable adsorption between PAHs and MGST.

The Freundlich model, an empirical equation, is usually used to describe adsorption on heterogeneous surface. K_F is Freundlich constant indicating adsorption capacity and n is an empirical parameter associated with the intensity of adsorption. The value of n will be in the range of 1–10 if the adsorption process is favorable. The values of K_F and n are collected in Table 1, the data of n also implies a favorable adsorption, being in accordance with that of R_L.

Table 1 Isotherm parameters of PAHs adsorption on MGST

	Langmuir				Freundlich		
	q_m (mg g^{-1})	K_L (L mg^{-1})	R_L	r^2	K_F (mg g^{-1})	n	r^2
NAP	27.00	0.1413	0.8762	0.9887	3.8710	1.4615	0.9890
PHE	60.44	0.2392	0.8070	0.9923	10.381	1.5081	0.9926
PYR	125.02	0.4815	0.6750	0.9976	73.565	1.2722	0.9983

All the Langmuir and Freundlich parameters are listed in Table 1. From the Table 1, it can be concluded from r^2 that the both models fit well with the adsorption and the Freundlich model fits the experimental data much better than that of Langmuir, indicating the presence of heterogeneous adsorption sites on the surface of MGST. It might be due to the defects in two-dimensional structure of MGST, which is illustrated in the Raman spectroscopy.

In view of adsorption capacity of MGST, the adsorption of PAHs has been compared and depicted in Fig. 4. It indicates that adsorption amount of PAHs has a rapid increase with increasing benzene number, i.e. PYR > PHE > NAY.

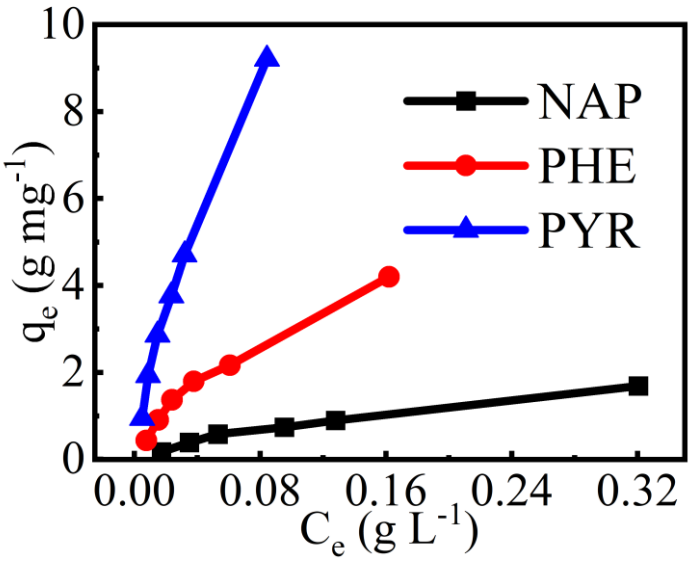

Fig. 4. The adsorption capacity of MGST for examined PAHs.

313 Additionally, the comparison of adsorption capacities of MGST estimated from the Langmuir
314 isotherm with those of reported various adsorbents were performed and the the results were
315 listed in Table 2. It is obvious that the q_m values of MGST are much higher than some of other
316 adsorbents, suggesting that MGST has a potential application in removing PAHs from the
317 wastewater.

318 **Table 2** Comparison of adsorption capacity of various adsorbents for PAHs

Adsorbent	Adsorption Capacity (mg g^{-1})			References
	NAP	PHE	PYR	
GNS	126±4.43	142±4.79	442±13.7	(Wang et al., 2014)
GO	3.67±0.143		6.39±0.146	
	7.81±0.116			
GO-9-AA	78.07	—	—	(Balati et al., 2017)
C60, Fullerene	2.3	—	—	(Cheng et al., 2004)
Multilayer Graphene	—	28.1	—	(Zhao et al., 2014)
Activated carbon	58.36	—	—	(Cabal et al., 2009)
RHAC	63.6	50.4	104.5	(Yakout et al., 2013)
MCAC-500W	189.43	—	—	(Ge et al., 2015)
MA-CAC	—	61.96	—	(Ge et al., 2016)
MGST	27.00	60.44	125.02	Present work

319 **2.1.6. Adsorption mechanism**

Analysis of the structure of MGST and PAHs, the π-π stacking, one type of electron donor-acceptor (EDA) interactions, is considered to be the main reason for the adsorption of PAHs by MGST. π-π EDA interaction is specific and non-covalent, which exists between electron-rich and electron-poor compounds (Yang et al., 2013). Since the π-electron depleted region of the MGST is mainly caused by surface defects and PAHs have the π-electron-rich aromatic rings, MGST can form π-π stacking with PAHs. This interaction has been used to interpret the adsorption of aromatic compounds on MGO (Kozlov et al., 2012).

2.1.7. Thermodynamic parameters

In order to examine the thermodynamic behavior of removal of PAHs by MGST, the thermodynamic parameters were estimated from these equations:

$$\Delta G^0 = -RT\ln K \tag{6}$$

$$\ln K = -\frac{\Delta H^0}{RT} + \frac{\Delta S^0}{R} \tag{7}$$

where R is the gas constant (8.314 J (mol K)$^{-1}$), T (K) the absolute temperature, K (q_e/C_e) the thermodynamic equilibrium constant at various temperatures.

Thermodynamic parameters evaluated at three temperatures have been given in Table 3. The negative values of ΔG^0 indicate that the adsorption is thermodynamically spontaneous, the decreasing of ΔG^0 with the rise of temperature states that the adsorption is more favorable at high temperatures. The positive ΔH^0 values suggest the adsorption is endothermic, and the positive values of ΔS^0 implies the increasing randomness at the solid/liquid interface during the adsorption of PAHs on MGST. At the same temperature, the ΔG_0 value is more negative with increasing number of benzene rings, and the values of ΔH_0 and ΔS_0 increase simultaneously. It corroborates that the adsorption is more favorable when the PAHs have more aromatic rings.

342

Table 3 Thermodynamic parameters of PAHs adsorption onto MGST at different temperatures

PAHs	$\Delta G/kJ \cdot mol^{-1}$			$\Delta H_0/kJ \cdot mol^{-1}$	$\Delta S_0/J \cdot mol^{-1} \cdot K^{-1}$
	298K	303K	313K		
NAP	-4.13	-4.84	-5.80	28.56	109.90
PHE	-8.07	-9.00	-10.14	32.05	134.99
PYR	-11.63	-12.69	-14.55	60.63	242.58

343 **2.2. Analysis of photodegradation**

344 In this study, photodegradation is applied to eliminate the adsorbed PAHs from MGST and
345 the photolysis process is monitored by GC-MS. There are five intermediates detected during
346 the photodegradation of naphthalene, including 1-naphthol (A), 1, 4-naphthalene quinone (B),
347 1,2-benzenedialdehyde (C), 1,2-benzenedicarboxylic acid (D) and 1,2-phenyldimethyl ester (E),
348 which is in accordance with the previous results (Farhadian et al., 2016; Yang et al., 2018). By
349 the EPR method, hydroxyl and superoxide radicals are captured in the photolysis (Fig. 5(a)).

350 Based on the results of EPR and GC-MS, the plausible degradation mechanism of
351 naphthalene is expressed in Fig. 6. The orbital wave function of naphthalene can be calculated
352 by Hückel molecular orbital method (HMO), then the free valence of each carbon can be
353 estimated (Fig. 5(b)). The reaction will occur at the carbon atom with a higher free valence.
354 Since the free valence of α carbon is larger than that of β carbon atom, α carbon is easily attacked
355 by hydroxyl or superoxide free radicals. In the photodegradation, ·OH radicals first attack α
356 carbon atom of naphthalene, then $\cdot O_2^-$ radicals react with the opposite carbon, and subsequently
357 release $\cdot HO_2^-$ and produce 1-naphthalenol. Another procedure may be as follows:
358 photogenerated pores directly oxidized naphthalene molecules to naphthalene cation radicals,

which interact with $\cdot O_2^-$ and decompose into 1, 4-naphthalene quinone (B). 1,2-benzenedialdehyde (C) might be obtained through the opening of aromatic ring and losing acetylene (C_2H_2), 1,2-benzenedialdehyde was further oxidized into 1,2-benzenedicarboxylic acid (D). And 1,2-benzenedicarboxylic acid (D) could be further become 1,2-phenyldimethyl ester (E). During the photolysis, $\cdot OH$ and $\cdot O_2^-$ species are responsible for the degradation of naphthalene.

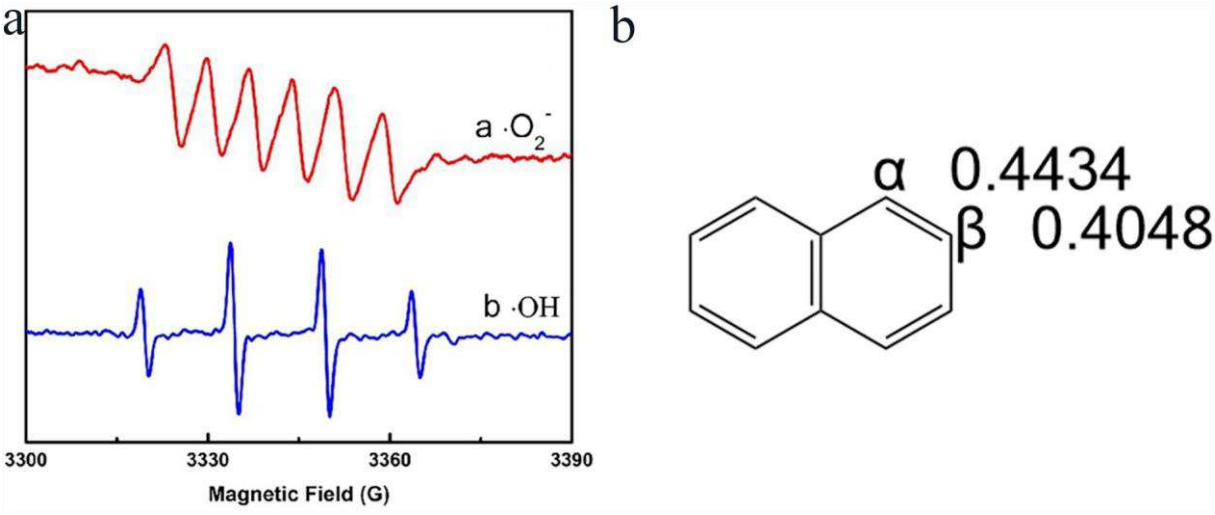

Fig. 5. DMPO spin-trapping EPR spectra of MGST in methanol (line-a) and in water (line-b) (a), the carbon position of the naphthalene molecule (b).

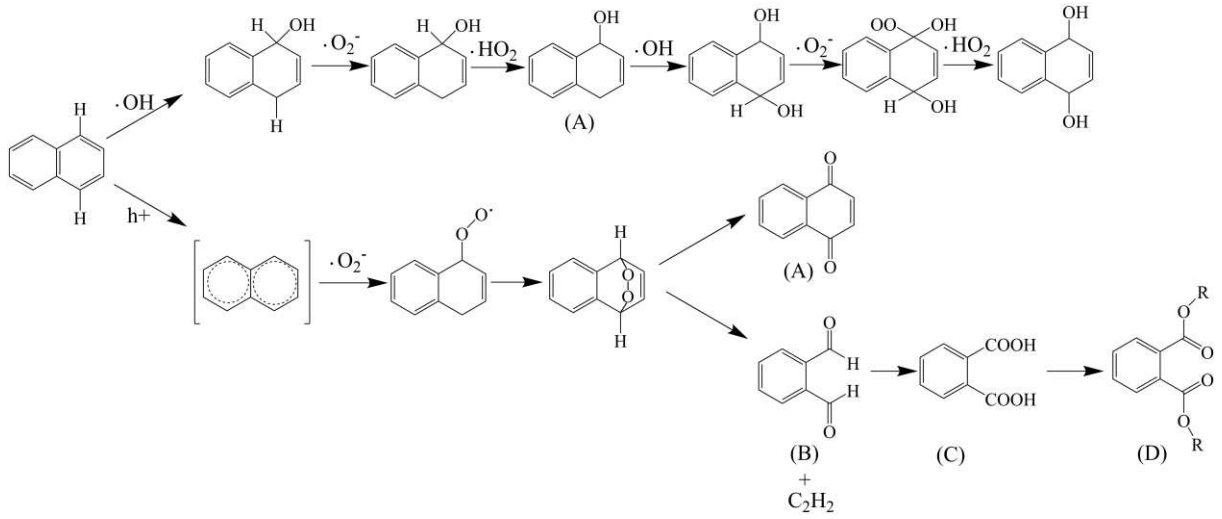

Fig. 6. Possible pathways for the formation of primary intermediates during the photodegradation of naphthalene.

2.3. Reusability of MGST

The reusability of adsorbent is of significance in practical water remediation. In this work, photolysis has been used as a desorption method to remove adsorbed PAHs and regenerate the adsorbent. The removal efficiencies of PAHs within five adsorption-desorption cycles are displayed in Fig. 7(a). In the five circles, the competitive adsorption efficiency of MGST follows the order of PYR > PHE > NAY and decreases slightly in the sequence of NAY > PHE > PYR. In these five desorption, photodegradation ratio is presented in Fig. 7(b), it is seen that the photolysis capability almost kept constant. This result is important and demonstrates that MGST has a good photocatalysis activity and can be regenerated by illumination. These results corroborate that MGST can be reused at least 5 times in successive removal processes without any significant loss in the adsorption and photodegrdation efficiency, showing its good sustainability.

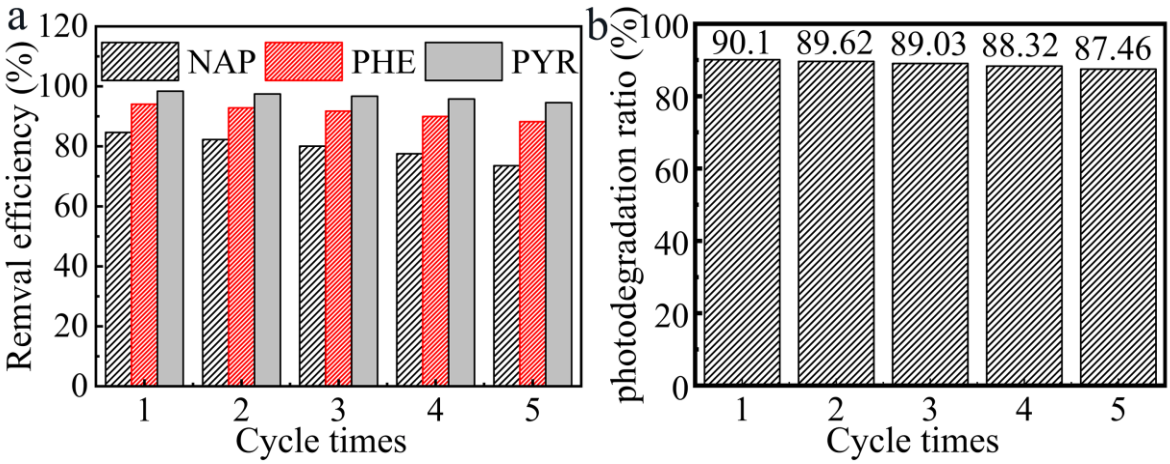

Fig. 7. The removal efficiency of MGST (a) and photodegradation ratio of NAP on MGST (b) during five cycles.

2.4. Real water matrix

It is known that many aromatic compounds exist in coking wastewater, the coking wastewater and tap water which spiked with 1.0 mg L^{-1} of PAHs were used to evaluate the effect of water matrix. The COD value of the coking wastewater is about 200. The experimental data in Table 4 indicates that the removal efficiency for overall aromatic compounds from coking wastewater is about 93% and the removal percentages for PAHs from tap water are above 80 %. This result demonstrates that the PAHs can be removed by MGST from different water matrix.

Table 4 Removal of PAHs from real water samples

	Coking plant wastewater	Tap water (pH 7.5)		
	(pH 8.5), COD(mg·L^{-1})	NAP (mg·L^{-1})	PHE (mg·L^{-1})	PYR (mg·L^{-})
Initial concentration	200	1	1	1
After adsorption	13. 76	0.188	0.091	0.045
Removal efficiency (%)	93.12	81.2	90.9	95.5

2.5. Material stability

In order to evaluate the stability of adsorbent, 20 mg MGST was put into 50 ml of aqueous solution of pH=2 for two weeks. The concentration of constituent elements of MGST in the solution was measured at different time intervals. From the data in Table S2, the leaching of Fe, Si and Ti are negligible, declaring that MGST has a good chemical stability.

3. Conclusion

Magnetic graphene oxide with photocatalytic ability (MGST) was synthesized for the sustainable treatment of PAHs. This adsorbent has been characterized by XRD, FTIR, Raman, SEM, TEM, VSM and XPS. Both adsorption and photodegradation were investigated in detail to understand the removal of PAHs by MGST. It has been found that MGST showed an efficient adsorption for PAHs (q_m for naphthalene, phenanthrene and pyrene is 27.00, 60.44 and 125.02 $mg \cdot g^{-1}$, respectively.), and had an encouraging photodegradation activity at the same time. Five intermediates were identified which suggested that the ·OH and $\cdot O_2^-$ radicals played a primary role in photodegradation of naphthalene. Additionally, regeneration experiment showed that there is no obvious decrease in the removal and photodegradation efficiency within five cycles. Overall, MGST could be applied in the environmental remediation because of its effective enrichment, easy separation, perfect photodegradation activity and durability.

Acknowledgements

The authors extend their appreciation to the National Natural Science Foundation of China.

Funding

This work was supported by the National Natural Science Foundation of China (No. 21776275, 21776012) and by the Key Program of National Natural Science Foundation of China (21838010).

Data availability

All data generated or analyzed during this study are included in this published article and its supplementary information files.

Author contribution

Qi Ying: synthesis of materials, investigation of materials, Adsorption and photocatalytic activity measurements, and writing of the original draft. Taiguang Li: interpretation of results and reviewing of the manuscript. Yongmei Hao: supervising the work. All authors read and approved the final manuscript

Declarations

Ethics approval and consent to participate: Not applicable.

Consent for publication: Not applicable.

Competing interests: The authors declare no competing interests.

Appendix A. Supplementary data

Supplementary data associated with this article can be found in online version at xxxxxx.

References

Balati, A., Ghanbari, M., Behzad, S.K., Amini, M.M., (2017) Functionalization of graphene oxide with 9-aminoanthracene for the adsorptive removal of persistent aromatic pollutants from aqueous solution. Acta Chim. Slov. 64: 479–490.

Benotti, M.J., Stanford, B.D., Wert, E.C., Snyder, S.A., (2009) Evaluation of a photocatalytic reactor membrane pilot system for the removal of pharmaceuticals and endocrine disrupting compounds from water. Water Res. 43: 1513–1522.

Cabal, B., Ania, C.O., Parra, J.B., Pis, J.J., (2009) Kinetics of naphthalene adsorption on an activated carbon: Comparison between aqueous and organic media. Chemosphere 76: 433–438.

Chen, F., Yang, Q., Zhong, Y., An, H., Zhao, J., Xie, T., et al., (2016) Photo-reduction of bromate in drinking water by metallic Ag and reduced graphene oxide (RGO) jointly modified $BiVO_4$ under visible light irradiation. Water Res. 101: 555–563.

Cheng, X., Kan, A.T., Tomson, M.B.,(2004) Naphthalene adsorption and desorption from aqueous C 60 fullerene. J. Chem. Eng. Data 49: 675–683.

Dappe, Y.J., Andersen, M., Balog, R., Hornekær, L., Bouju, X., (2015) Adsorption and STM imaging of polycyclic aromatic hydrocarbons on graphene. Phys. Rev. B - Condens. Matter Mater. Phys. 91: 1–8.

Farhadian, M., Sangpour, P., Hosseinzadeh, G., (2016) Preparation and photocatalytic activity of WO_3-MWCNT nanocomposite for degradation of naphthalene under visible light irradiation. RSC Adv. 6: 39063–39073.

Gao, J., Huang, C., Lin, Y., Tong, P., Zhang, L., (2016) In situ solvothermal synthesis of metal-organic framework coated fiber for highly sensitive solid-phase microextraction of polycyclic aromatic hydrocarbons. J. Chromatogr. A 1436: 1–8.

Ge, X., Tian, F., Wu, Zhilin, Yan, Y., Cravotto, G., Wu, Zhansheng, (2015) Adsorption of naphthalene from aqueous solution on coal-based activated carbon modified by microwave induction: Microwave power effects. Chem. Eng. Process. Process Intensif. 91: 67–77.

Ge, X., Wu, Zhansheng, Wu, Zhilin, Yan, Y., Cravotto, G., Ye, B.C., (2016) Microwave-assisted modification of activated carbon with ammonia for efficient pyrene adsorption. J. Ind. Eng. Chem. 39: 27–36.

Glomstad, B., Altin, D., Sørensen, L., Liu, J., Jenssen, B.M., Booth, A.M., (2016) Carbon Nanotube Properties Influence Adsorption of Phenanthrene and Subsequent Bioavailability and Toxicity to Pseudokirchneriella subcapitata. Environ. Sci. Technol. 50: 2660–2668.

Goswami, L., Manikandan, N.A., Dolman, B., Pakshirajan, K., Pugazhenthi, G., (2018) Biological treatment of wastewater containing a mixture of polycyclic aromatic hydrocarbons using the oleaginous bacterium Rhodococcus opacus. J. Clean. Prod. 196: 1282–1291.

Gupta, S., Pathak, B., Fulekar, M.H., (2015) Molecular approaches for biodegradation of polycyclic aromatic hydrocarbon compounds: a review. Rev. Environ. Sci. Biotechnol. 14: 241–269.

Hao, Y.M., Man, C., Hu, Z.B., (2010) Effective removal of Cu (II) ions from aqueous solution by amino-functionalized magnetic nanoparticles. J. Hazard. Mater. 184: 392–399.

Huang, Y., Zhang, W., Ruan, G., Li, X., Cong, Y., Du, F., et al., (2018) Reduced Graphene Oxide-Hybridized Polymeric High-Internal Phase Emulsions for Highly Efficient Removal of Polycyclic Aromatic Hydrocarbons from Water Matrix. Langmuir 34: 3661–3668.

Hung, C.M., Huang, C.P., Lam, S.S., Chen, C.W., Dong, C. Di, (2020) The removal of polycyclic aromatic hydrocarbons (PAHs) from marine sediments using persulfate over a nano-sized iron composite of magnetite and carbon black activator. J. Environ. Chem. Eng. 8: 104440.

Junyong, C., Yongmei, H., Yan, L., Jiajia, G., (2013) Magnetic graphene oxides as highly effective adsorbents for rapid removal of a cationic dye rhodamine B from aqueous solutions. RSC Adv. 3: 7254–7258.

505 Ji, W., Zhang, M., Duan, W., Wang, X., Zhao, H., Guo, L., et al., (2017) Insight into the
506 highly efficient degradation of PAHs in water over graphene oxide/Ag_3PO_4 composites
507 under visible light irradiation. Chem. Eng. J. 334: 104–110.
508 Kozlov, S.M., Viñes, F., Görling, A., (2012) On the interaction of polycyclic aromatic
509 compounds with graphene. Carbon. 50: 2482–2492.
510 Marcano, D.C., Kosynkin, D. V, Berlin, J.M., Sinitskii, A., Sun, Z., Slesarev, A., et al., (2010)
511 ACS Nano. 4: 4806–4814.
512 Oliveira, R.V.M., Lima, J.R.A., Cunha, G. da C., Romão, L.P.C., (2020) Use of eco-friendly
513 magnetic materials for the removal of polycyclic aromatic hydrocarbons and metals from
514 environmental water samples. J. Environ. Chem. Eng. 8: 104050.
515 Purcaro, G., Moret, S., Conte, L.S., (2013) Overview on polycyclic aromatic hydrocarbons:
516 Occurrence, legislation and innovative determination in foods. Talanta 105: 292–305.
517 Sheikhmohammadi, A., Safari, M., Alinejad, A., Esrafili, A., Nourmoradi, H., Asgari, E.,
518 (2019) The synthesis and application of the Fe_3O_4@SiO_2 nanoparticles functionalized
519 with 3-aminopropyltriethoxysilane as an efficient sorbent for the adsorption of
520 ethylparaben from wastewater: Synthesis, kinetic, thermodynamic and equilibrium
521 studies. J. Environ. Chem. Eng. 7: 2213-3437.
522 Shen, J.H., Li, M.M., Chu, L.F., Guo, C.X., Guo, Y.J., Guo, Y.P., (2021) Effect mechanism
523 of copper ions on photocatalytic activity of TiO2/graphene oxide composites for phenol-
524 4-sulfonic acid photodegradation. J. Colloid Interface Sci. 586: 563–575.
525 Sun, Y., Yang, S., Zhao, G., Wang, Q., Wang, X., (2013) Adsorption of polycyclic aromatic
526 hydrocarbons on graphene oxides and reduced graphene oxides. Chem. - An Asian J. 8:
527 2755–2761.
528 Vidal, C.B., Barros, A.L., Moura, C.P., de Lima, A.C.A., Dias, F.S., Vasconcellos, L.C.G., et
529 al., (2011) Adsorption of polycyclic aromatic hydrocarbons from aqueous solutions by
530 modified periodic mesoporous organosilica. J. Colloid Interface Sci. 357: 466–473.
531 Wang, H., Hao, Q., Yang, X., Lu, L., Wang, X., (2009) Graphene oxide doped polyaniline for
532 supercapacitors. Electrochem. commun. 11: 1158–1161.
533 Wang, J., Chen, Z., Chen, B., (2014) Adsorption of polycyclic aromatic hydrocarbons by
534 graphene and graphene oxide nanosheets. Environ. Sci. Technol. 48: 4817–4825.

Wickramasinghe, A.D.L., Shukla, S.P., (2018) Performance evaluation of a pellet based column bed for removal of a potentially carcinogenic Polycyclic Aromatic Hydrocarbon (PAH) from water. J. Environ. Chem. Eng. 6: 6012–6020.

Xi, Z., Chen, B., (2014) Removal of polycyclic aromatic hydrocarbons from aqueous solution by raw and modified plant residue materials as biosorbents. J. Environ. Sci. (China) 26: 737–748.

Yakout, S.M., Daifullah, A.A.M., El-Reefy, S.A., (2013) Adsorption of naphthalene, phenanthrene and pyrene from aqueous solution using low-cost activated carbon derived from agricultural wastes. Adsorpt. Sci. Technol. 31: 293–302.

Yang, X., Cai, H., Bao, M., Yu, J., Lu, J., Li, Y., (2018) Insight into the highly efficient degradation of PAHs in water over graphene oxide/Ag_3PO_4 composites under visible light irradiation. Chem. Eng. J. 334: 355–376.

Yang, X., Li, J., Wen, T., Ren, X., Huang, Y., Wang, X., (2013) Adsorption of naphthalene and its derivatives on magnetic graphene composites and the mechanism investigation. Colloids Surfaces A Physicochem. Eng. Asp. 422: 118–125.

Ying, Q., Hao, Y., Wang, Z., Li, X., (2019) Facile one-step preparation of triethanolamine modified magnetic nanoparticles for the high-efficient removal of Cu (II) ions and methylene blue. J. Taiwan Inst. Chem. Eng. 95: 32–39.

Yu, K., Huang, L., Lou, L.L., Chang, Y., Dong, Y., Wang, H., et al., (2015) Degradation of polycyclic aromatic hydrocarbons in crumb tyre rubber catalysed by rutile TiO_2 under UV irradiation. Environ. Technol. (United Kingdom) 36: 1008–1015.

Zhang, Caili, Wu, L., Cai, D., Zhang, Caiyun, Wang, N., Zhang, J., et al., (2013) Adsorption of polycyclic aromatic hydrocarbons (fluoranthene and anthracenemethanol) by functional graphene oxide and removal by pH and temperature-sensitive coagulation. ACS Appl. Mater. Interfaces 5: 4783–4790.

Zhao, J., Wang, Z., Zhao, Q., Xing, B., (2014) Adsorption of phenanthrene on multilayer graphene as affected by surfactant and exfoliation. Environ. Sci. Technol. 48: 331–339.

Supplementary Files

This is a list of supplementary files associated with this preprint. Click to download.

- GraphicalAbstract.docx
- Supplementarymaterials.docx